Inorganic Chemistry
Article
pubs.acs.org/IC

Electrocatalytic Reduction of CO_2 to CO With Re-Pyridyl-NHCs: Proton Source Influence on Rates and Product Selectivities

Nalaka P. Liyanage, Hunter A. Dulaney, Aron J. Huckaba, Jonah W. Jurss,* and Jared H. Delcamp*

Department of Chemistry and Biochemistry, University of Mississippi, Coulter Hall, University, Mississippi 38677, United States

Ⓢ *Supporting Information*

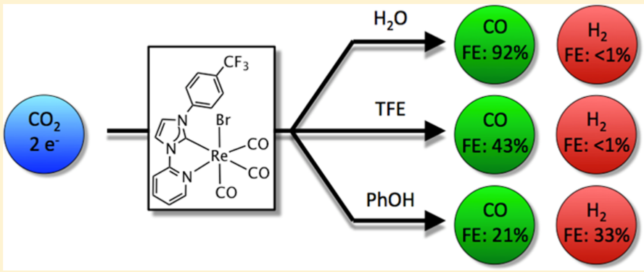

ABSTRACT: A series of four electron-deficient-substituted Re(I) pyridyl *N*-heterocyclic carbene (pyNHC) complexes have been synthesized, and their electrocatalytic reduction of CO_2 has been evaluated by cyclic voltammetry and controlled potential electrolysis experiments. All of the catalysts were evaluated by cyclic voltammetry under inert atmosphere and under CO_2 and compared to the known benchmark catalyst Re(bpy)$(CO)_3$Br. Among the four Re-NHC catalysts, Re-(pyNHC-PhCF_3)$(CO)_3$Br (**2**) demonstrated the highest catalytic rate $(i_{cat}/i_p)^2$ at the first and second reduction events with a value of 4 at the second reduction potential (TOF = 0.8 s^{-1}). The rate of catalysis was enhanced through the addition of proton sources (PhOH, TFE, and H_2O; TOF up to 100 s^{-1}; $(i_{cat}/i_p)^2 = 700$). Controlled potential electrolysis shows Faradaic efficiencies (FE) for CO production and accumulated charge for the Re(pyNHC-PhCF_3)$(CO)_3$Br catalyst exceed those of the benchmark catalyst in the presence of 2 M H_2O (92%, 13 C at 1 h versus 61%, 3 C for the benchmark catalyst) under analogous experimental conditions. A peak FE of 100% was observed during electrolysis with Re(pyNHC-PhCF_3)$(CO)_3$Br.

■ INTRODUCTION

Efficient catalytic conversion of CO_2 is a critical need with many reduced products, including CO, having potential fuel uses.[1−5] One electron reduction of CO_2 to $CO_2^{\bullet-}$ is an energetically demanding process (−1.97 V vs NHE in DMF); however, multiple electron reduction pathways are available at substantially lower potentials (HCO_2H at −0.61 V, CO at −0.53 V, HCHO at −0.48 V, CH_3OH at −0.38 V, and CH_4 at −0.24 V vs NHE).[6] The use of a catalyst to facilitate the multielectron reduction of CO_2 is useful in overcoming slow rates, minimizing the overpotential required for catalysis, and controlling product selectivities.[7−23]

Recently, we demonstrated the photocatalytic activity of a Re-NHC-based catalyst for the conversion of CO_2 to CO under solar-simulated irradiation and found electron-withdrawing substituents improved catalysis.[11] The Re(PyNHC-PhCF_3)-$(CO)_3$Br catalyst reported therein was briefly analyzed via cyclic voltammetry for electrocatalytic CO_2 reduction. Interestingly, a catalytic current increase was observed at the first reduction potential, which could lead to lower overpotentials when compared to many Re-based catalysts that reduce CO_2 at the second reduction potential.[20,24,25] We hypothesized that the electron-rich nature of the NHC ligand allows for the donation of an electron from the NHC motif in addition to the electron on the reduced complex to deliver two electrons to CO_2 as is required for the CO production observed (Figure 1). While the addition of an electron-rich NHC ring in place of a pyridine group increases the energy required for the first reduction, catalysis at the first reduction potential rather than the second reduction potential may lead to overall lower overpotentials for catalysis. With the goals of lowering overpotentials and evaluating catalytic rate effects, we sought to introduce strongly electron-withdrawing substituents near the NHC ring. Herein, we report analysis of the electrocatalytic properties of the Re(PyNHC-PhCF_3)$(CO)_3$Br catalyst under various conditions and the effect on catalysis by varying electron-withdrawing groups (−NO_2, −CN, bis(CF_3)) on the NHC-aryl substituent.

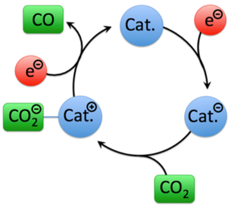

Figure 1. A general proposed scheme for the electrocatalytic conversion of CO_2 to CO, where a Re(L) catalyst reduces CO_2 after the first reduction of the catalyst. Two proton transfers are understood with an added proton source, but are not explicitly denoted when they occur above.

Our previous studies have shown that an electron-withdrawing trifluoromethyl group on the pyridyl *N*-heterocyclic carbene (PyNHC) ligand promotes photocatalysis and modestly reduces overpotentials in electrocatalysis. Encouraged by these results, we have targeted catalysts with different electron-withdrawing substituents in place of the PhCF_3 group on Re(pyNHC-PhCF_3)$(CO)_3$Br (**2**), including *p*-PhNO_2 (**3**),

Received: March 11, 2016

DOI: 10.1021/acs.inorgchem.6b00626

p-PhCN (**4**), and Ph*bis*(*m*-CF_3) (**5**), to study the effects of these electron-withdrawing groups on electrocatalytic overpotentials and rates (Figure 2). Catalysts **3** and **4** were selected to evaluate the effects of resonance active electron-withdrawing groups, while catalysts **2** and **5** incorporate strong inductively withdrawing substituents.

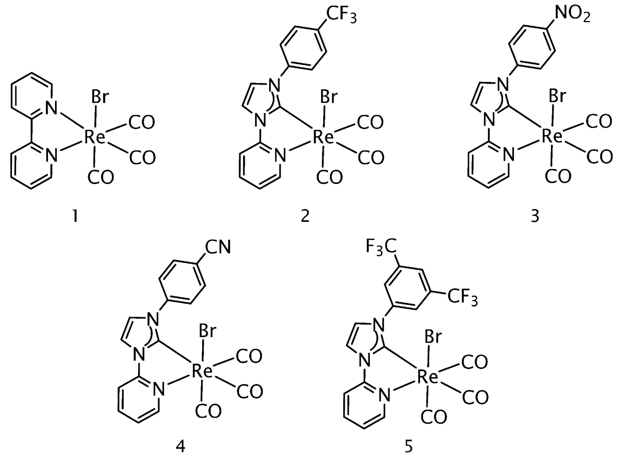

Figure 2. Structures of benchmark Re(bpy)$(CO)_3$Br (**1**) and target Re(pyNHC-aryl) catalysts (**2**−**5**) with variable electron-withdrawing groups on the pyNHC-aryl ligand (**2**−**5**).

■ EXPERIMENTAL SECTION

General Information. All commercially obtained reagents were used as received. Unless otherwise noted, all of the reactions were conducted under a N_2 atmosphere. Thin-layer chromatography (TLC) was conducted with sigma T-6145 precoated TLC silica gel 60 F_{254} polyester sheets and visualized with UV and potassium permanganate staining. Flash column chromatography was performed with SilicaFlash P60, 40−63 μm (230−400 mesh). ^1H NMR spectra were recorded on a Bruker Avance-300 (300 MHz), Bruker Avance DRX-500 (500 MHz) spectrometer, and reported in ppm using solvent as an internal standard ($CDCl_3$ at 7.26 ppm). Data were reported as s = singlet, d = doublet, t = triplet, q = quartet, p = pentet, m = multiplet, b = broad, ap = apparent; coupling constants were in hertz. Compounds **6**−**11** are commercially available. 4-(1*H*-Imidazol-1-yl)benzonitrile (**12**) is available via a previously reported procedure.[26] 1-(3,5-Bis(trifluoromethyl)phenyl)-1*H*-imidazole (**13**) is available via a previously reported procedure.[27] Syntheses of 3-(pyridin-2-yl)-1-(4-(trifluoromethyl)phenyl)-1*H*-imidazol-3-ium bromide (**14**) and fac-{3-(4-trifluoromethylphenyl)-1-(2′-pyridyl)imidazolin-2-ylidene} tricarbonylbromorhenium(I) (**2**) are available through previously reported procedures; however, an improved synthetic protocol for **14** is given below.[11] Additional experimental information on cyclic voltammetry experiments, controlled potential electrolysis experiments, additional electrochemical data, and NMR data is available via the Supporting Information. All potential values are reported versus NHE (Fc/Fc^+ = 0.4 V vs SCE; SCE − 0.24 V = NHE).[36]

*3-(Pyridin-2-yl)-1-(4-(trifluoromethyl)phenyl)-1H-imidazol-3-ium Bromide (**14**).* Into a flame-dried flask connected to a reflux condenser were added 1-(4-(trifluoromethyl)phenyl)-1*H*-imidazole (**10**) (200 mg, 0.94 mmol), 2-bromopyridine (0.18 mL, 1.88 mmol), and anhydrous DMF (1 mL). The mixture then was degassed with N_2 for 30 min and stirred with reflux under a N_2 atmosphere. After 2 days, the reaction mixture was cooled to room temperature to form a solid. The filtered solid was dissolved in dichloromethane and reprecipitated with diethyl ether to give a brown microcrystalline solid (99%). ^1H NMR (300 MHz, $CDCl_3$): δ 12.47 (s, 1H), 9.33 (d, *J* = 7.9 Hz, 1H), 8.58−8.38 (m, 2H), 8.37 (d, *J* = 8.0, 2H), 8.17−8.13 (m, 1H), 7.95 (d, *J* = 8.0 Hz, 2H), 7.79 (s, 1H), 7.55−7.51 (m, 1H) ppm.

*1-(4-Nitrophenyl)-3-(pyridin-2-yl)-1H-imidazol-3-ium Bromide (**15**).* Into a flame-dried pressure vial were added 1-(4-nitrophenyl)-1*H*-imidazole (**11**) (250 mg, 1.32 mmol) and 2-bromopyridine (0.25 mL, 2.64 mmol). The neat mixture was stirred at 175 °C, and the reaction was monitored using ^1H NMR. After 1 day the reaction mixture was cooled to room temperature to form a solid. The filtered solid was dissolved in 1% methanol:dichloromethane and reprecipitated with diethyl ether to give a brown microcrystalline solid (96%). ^1H NMR (500 MHz, $CDCl_3$): δ 12.73 (s, 1H), 7.35 (d, *J* = 3.6, 1H), 8.60−8.48 (m, 6H), 8.17 (t, *J* = 7.6, 1H), 7.79 (s, 1H), 7.55 (dd, *J* = 4.7, 3.1 Hz, 1H) ppm. ^{13}C NMR (125 MHz, DMSO): δ 149.9, 148.4, 146.6, 141.2, 139.6, 135.8, 126.2, 126.0, 124.0, 122.7, 120.7, 115.3 ppm. IR (neat, cm^{-1}): 3080, 3015, 1555, 1525, 1290, 854, 780, 745. HRMS (ESI) *m*/*z* calculated for $C_{14}H_{11}N_4O_2^+$ ($[M - Br]^+$) 267.0882, found 267.0872.

*1-(4-Cyanophenyl)-3-(pyridin-2-yl)-1H-imidazol-3-ium Bromide (**16**).* Into a flame-dried pressure vial were added **12** (250 mg, 1.32 mmol) and 2-bromopyridine (0.30 mL, 2.96 mmol). The neat mixture was stirred at 175 °C, and the reaction was monitored using ^1H NMR. After 1 day the reaction mixture was cooled to room temperature to form a solid. The filtered solid was dissolved in dichloromethane and reprecipitated with diethyl ether to give a brown microcrystalline solid (83%). ^1H NMR (300 MHz, DMSO-d_6): δ 10.76 (s, 1H), 8.80 (s, 1H), 8.73 (d, *J* = 4.6 Hz, 1H), 8.68 (s, 1H), 8.33−8.18 (m, 6H), 7.72 (dd, *J* = 5.0, 2.1, 1H) ppm. ^{13}C NMR (125 MHz, DMSO): δ 149.8, 146.6, 141.2, 138.3, 135.5, 134.8, 126.17, 123.6, 122.5, 120.7, 118.3, 115.4, 113.1 ppm. IR (neat, cm^{-1}): 3045, 3010, 2224, 1602, 1545, 1469, 1436, 1262, 841, 782. HRMS (ESI) *m*/*z* calculated for $C_{15}H_{11}N_4^+$ ($[M - Br]^+$) 247.0984, found 247.0943.

*1-(3,5-Bis(trifluoromethyl)phenyl)-3-(pyridin-2-yl)-1H-imidazol-3-ium Bromide (**17**).* Into a flame-dried flask connected to the reflux condenser were added **13** (200 mg, 0.71 mmol) and 2-bromopyridine (0.14 mL, 1.43 mmol), DMF (~1 mL), then it was stirred to reflux, and the reaction was monitored using ^1H NMR. After 2 days, the reaction mixture was cooled to rt to form a solid. The solid then was dissolved in dichloromethane and reprecipitated with ether to give a brown microcrystalline solid (81%). ^1H NMR (500 MHz, $CDCl_3$): δ 12.55 (s, 1H), 9.21 (d, *J* = 8.3 Hz, 1H), 8.72 (s, 2H), 8.63 (t, *J* = 1.6 Hz, 1H), 8.57 (dd, *J* = 3.7 Hz, 1H), 8.15−8.12 (m, 1H), 8.10 (s, 1H), 7.92 (s, 1H), 7.54 (dd, *J* = 4.5, 2.7 Hz, 1H) ppm. ^{13}C NMR (125 MHz, $CDCl_3$): δ 149.9, 146.6, 141.3, 136.6, 136.1, 132.4, 132.1, 126.3, 124.6, 124.3, 123.2, 122.1, 120.4, 115.2 ppm. IR (neat, cm^{-1}): 3151, 3010, 2942, 2827, 2249, 1595, 1364, 1279, 1126. HRMS (ESI) *m*/*z* calculated for $C_{16}H_{10}F_6N_3^+$ ($[M - Br]^+$) 358.0779, found 358.0727.

*fac-{3-(4-Nitrophenyl)-1-(2′-pyridyl)imidazolin-2-ylidene} Tricarbonylbromorhenium(I) (**3**).* To a flame-dried flask equipped with a reflux condenser were added **15** (0.1 g, 0.29 mmol), $Re(CO)_5Br$ (0.12 g, 0.29 mmol), triethylamine (0.4 mL, 2.88 mmol), and anhydrous, degassed toluene (5 mL). The mixture was refluxed under a N_2 atmosphere overnight. The reaction mixture then was cooled to room temperature, and toluene was removed under reduced pressure. The crude product was purified through silica gel column by using 2% acetone:ethyl acetate to give a yellow crystalline solid of **3** (40%). The isolated compound was found to immediately change color upon standing to a green-brown color. ^1H NMR (300 MHz, $CDCl_3$): δ 8.96 (d, *J* = 4.6 Hz, 1H), 8.48 (d, *J* = 8.8 Hz, 2H), 8.13−8.07 (m, 1H), 7.97 (d, *J* = 8.9 Hz, 2H), 7.82 (d, *J* = 1.9 Hz, 1H), 7.70−7.68 (m, 1H), 7.42−7.36 (m, 2H) ppm. IR (neat, cm^{-1}): 2956, 2925, 2856, 2362, 2336, 2018, 1920, 1892, 1612, 1526, 1487, 1346. HRMS (ESI) *m*/*z* calculated for $C_{17}H_{10}BrN_4O_5ReCs$ ($[M + Cs]^+$) 748.8429, found 748.8687.

*fac-{3-(4-Cyanophenyl)-1-(2′-pyridyl)imidazolin-2-ylidene} Tricarbonylbromorhenium(I) (**4**).* To a flame-dried flask equipped with a reflux condenser were added **16** (0.04 g, 0.123 mmol), $Re(CO)_5Br$ (0.05 g, 0.123 mmol), triethylamine (0.2 mL, 1.23 mmol), and anhydrous, degassed toluene (2 mL). The mixture was refluxed under a N_2 atmosphere overnight. The reaction mixture then was cooled to room temperature, and toluene was removed under reduced pressure. The crude product was purified through a silica gel plug by using ethyl acetate → 2% acetone:ethyl acetate to give a pale yellow

Scheme 1. Synthetic Route To Obtain Desired Re(pyNHC-aryl)$(CO)_3Br$ Catalysts 2−5[a]

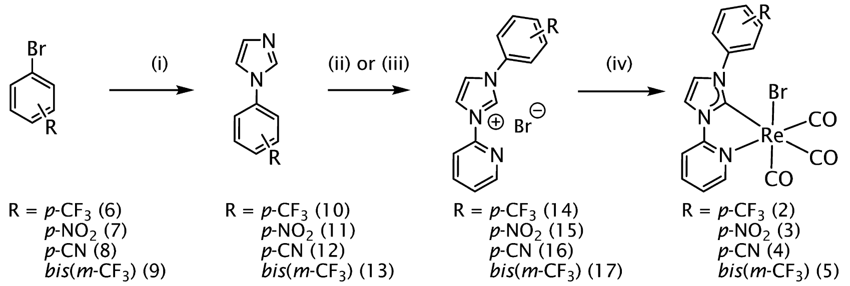

[a] Reaction conditions: (i) CuI, imidazole, K_3PO_4, DMF, 130 °C, yields, **10** commercial, **11** commercial, **12** 14%, **13** 88%; (ii) 2-bromopyridine, DMF, reflux, yields, **14** 99%, **17** 81%; (iii) 2-bromopyridine, 160 °C, yields, **15** 96%, **16** 34%; (iv) $Re(CO)_5Br$, NEt_3, toluene, reflux, yields, **2** 56%, **3** 40%, **4** 95%, **5** 36%.

crystalline solid of **4** (95%). ^1H NMR (300 MHz, acetone-d_6): δ 9.02 (d, J = 4.7 Hz, 1H), 8.57 (d, J = 2.0 Hz, 1H), 8.41−8.31 (m, 2H), 8.15−8.06 (m, 4H), 7.95 (d, J = 2.2 Hz, 1H), 7.64−7.60 (m, 1H) ppm. ^{13}C NMR (75 MHz, CD_3CN): δ 197.1, 196.0, 192.2, 188.1, 153.6, 152.9, 142.9, 142.0, 134.4, 133.9, 127.7, 124.5, 124.1, 123.0, 117.5, 113.2 ppm. IR (neat, cm^{-1}): 2925, 2856, 2233, 2017, 1918, 1890, 1611, 1487, 1427, 1318. HRMS (ESI) m/z calculated for $C_{18}H_{10}BrN_4O_3ReCs$ ($[M + Cs]^+$) 728.8531, found 728.8516.

*fac-{3-(3,5-Bis(trifluoromethyl)phenyl)-1-(2′-pyridyl)imidazolin-2-ylidene} Tricarbonylbromorhenium(I) (**5**).* To a flame-dried flask equipped with a reflux condenser were added **17** (0.051 g, 0.123 mmol), $Re(CO)_5Br$ (0.05 g, 0.123 mmol), triethylamine (0.2 mL, 1.23 mmol), and anhydrous, degassed toluene (2 mL). The mixture was refluxed under a N_2 atmosphere overnight. The reaction mixture then was cooled to room temperature, and toluene was removed under reduced pressure. The crude product was dissolved in dichloromethane and precipitated by adding diethyl ether to give a pale yellow crystalline solid of **5** (36%). ^1H NMR (300 MHz, $CDCl_3$): δ 8.98 (d, J = 5.3 Hz, 1H), 8.29 (s, 2H), 8.15−8.09 (m, 2H), 7.82 (s, 1H), 7.69 (d, J = 8.2 Hz, 1H), 7.42−7.35 (m, 2H) ppm. ^{13}C NMR (125 MHz, CD_3CN): δ 197.0, 196.5, 192.9, 188.0, 153.7, 152.9, 142.0, 140.8, 132.6, 132.2, 128.0, 124.7, 124.2, 123.6, 121.9, 118.0, 113.3 ppm. IR (neat, cm^{-1}): 2940, 2666, 2361, 2336, 2018, 1919, 1892, 1614, 1474, 1279, 1179, 1138. HRMS (ESI) m/z calculated for $C_{19}H_9BrF_6N_3O_3ReCs$ ($[M + Cs]^+$) 839.8326, found 839.8410.

RESULTS AND DISCUSSION

Catalyst Synthesis. The synthesis of Re(PyNHC) complexes is well-established with several reported protocols available.[28−30] In this study, we utilized known procedures to rapidly generate the target catalysts (Scheme 1). Briefly, the synthesis of catalysts **2**−**5** starts with a Cu(I)-catalyzed coupling of commercially available imidazole to the appropriately substituted phenyl bromide (**6**−**9**) to obtain compounds **10**−**13** (Scheme 1). Heating **10**−**13** with neat 2-bromopyridine gives intermediates **14**−**17** by nucleophilic aromatic substitution in moderate to excellent yields. This procedure gave reduced yields of **14** and **17** (<10%) due to sublimation of **10** and **13**. However, addition of a solvent (DMF) and refluxing the 2-bromopyridine with aryl imidazole gave the desired **14** and **17** in high yield (>80%). Soft deprotonation of the imidazolium salt in the presence of $Re(CO)_5Br$ and triethylamine gave the final catalysts **2**−**5** in excellent to moderate yields (95%−35%). Notably, purification of all catalysts was performed in air by silica gel chromatography. Of this series, only catalyst **3** was not amenable to these conditions as decomposition was observed in going from a yellow to darker green solid in solutions open to air on the time scale of minutes.

Electrochemical Studies. With catalysts **2**−**5** in hand, cyclic voltammetry was performed to determine the reduction potentials of each system under N_2. The thermodynamic potential for CO_2 reduction to CO has been estimated to be around −0.5 V (vs NHE) in the presence of carbonic acid formed from CO_2 and H_2O as the strongest acid in solution with an assumed pK_a of 17 in acetonitrile.[11,14,31,32] We stress that this value is only an estimate as the value has been derived through thermodynamic cycles with inputs from the Nernst equation or DFT calculations. Our experiments throughout this article are not performed under buffered conditions (1:1 acid:conjugate acid), which will clearly effect the estimated standard reduction potential.[33] However, an estimate of this potential is useful when evaluating the potential utility of new catalysts. With a reduction potential more negative than −0.5 V vs NHE, catalytic activity is estimated to be thermodynamically favored. The measured onset of the first reduction potentials of **2**−**5** occurs over a narrow range from approximately −1.25 to −1.30 V vs NHE (Table 1). The second reduction potentials were again found to vary by approximately 50 mV from −1.70 to −1.75 V vs NHE, which illustrates modest tunability of the catalyst reduction potentials by modifications to the aryl group substituent. Catalyst **2** appears to have the lowest energy reduction potential for the first wave, while catalyst **5** has the lowest energy reduction potential for the second wave. The

Table 1. Cyclic Voltammetry Properties of Catalysts 2−5 under N_2 and CO_2[a]

catalyst	$E_{(s/s-)}$ (V)	$E_{(s-/s2-)}$ (V)	$(i_{cat1}/i_{p1})^2$	TOF (s^{-1}) peak 1	$(i_{cat2}/i_{p2})^2$	TOF (s^{-1}) peak 2
1	−0.95	−1.30	1	0.3	10	2
2	−1.25	−1.75	3	0.6	4	0.8
4	−1.30	−1.75	2	0.3	2	0.3
5	−1.30	−1.70	2	0.4	2	0.4

[a] All estimated reduction wave onset values are reported versus NHE under N_2 and rounded to the nearest 0.05 V. Values are measured in MeCN (1 mM cat.), 0.1 M n-Bu_4NPF_6 electrolyte with a glassy carbon working electrode, platinum counter electrode and platinum pseudo-reference electrode with ferrocene as the internal standard. All the scans are performed at 100 mV/s. i_{cat1} and i_{cat2} are the peak catalytic currents at the first and second reduction waves under a CO_2 atmosphere, respectively. i_p is the peak current under an N_2 atmosphere and is denoted as the first or second reduction peak. Given the deviation from ideal S-shaped curves in the cyclic voltammetry measurements all $(i_{cat}/i_p)^2$ values and all TOF values are estimates of catalytic rates and are reported to a single significant figure throughout this manuscript.[34]

DOI: 10.1021/acs.inorgchem.6b00626
Inorg. Chem. XXXX, XXX, XXX−XXX

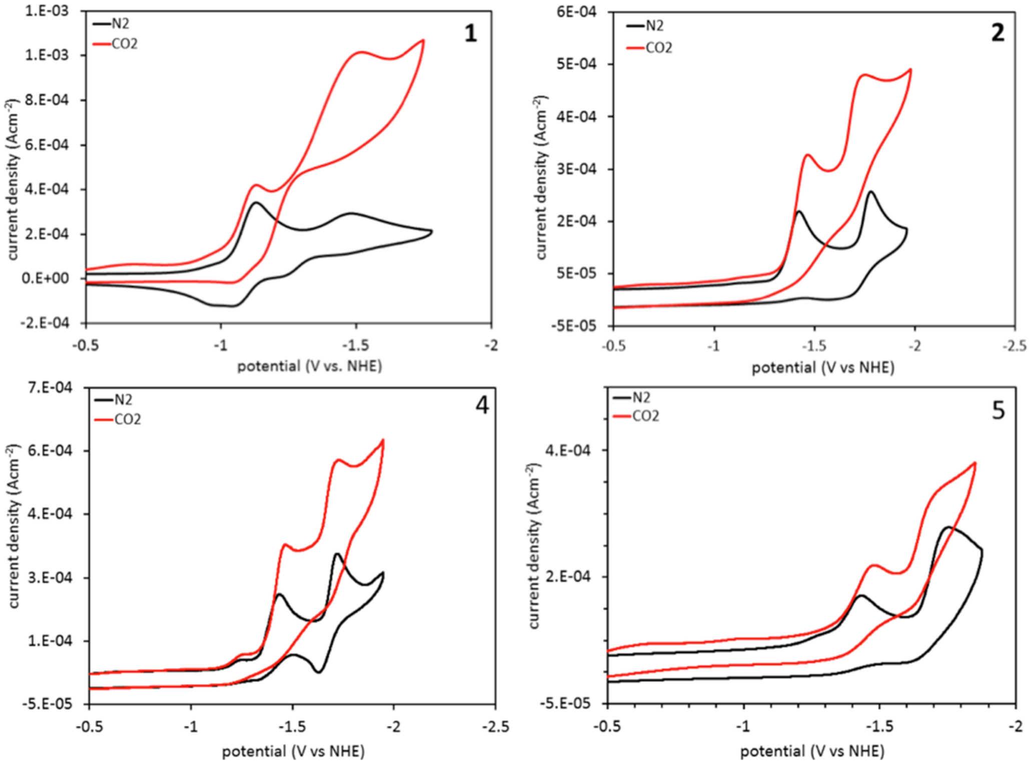

Figure 3. CV curves for the catalysts **1**−**2** and **4**−**5**, measured in acetonitrile with 0.1 M *n*-Bu_4NPF_6 electrolyte under N_2 (black) and CO_2 (red) atmosphere. Glassy carbon working electrode, platinum counter electrode, and platinum pseudoreference electrodes are used for the measurements with ferrocene as the internal standard and a scan rate of 100 mV/s. All potential values are reported versus NHE (Fc/Fc^+ = 0.4 V vs SCE; SCE − 0.24 V = NHE).[36]

values are estimated from onset reduction potentials as the first and second reductions are irreversible under these conditions. Catalyst **3** was found to be unstable in solution, and decomposition was evident in the CV before a single scan could be obtained (Figure S1). The solution stable catalysts were all found to have thermodynamically favorable reduction potentials for the 2-electron reduction of CO_2 to CO. Comparing NHC-catalysts **2**, **4**, and **5** with benchmark bipyridyl catalyst **1**, both the first and the second reduction potential onsets vary by 300−350 mV more negative relative to catalyst **1**.

All estimated reduction wave onset values are reported versus NHE under N_2 and rounded to the nearest 0.05 V. Values are measured in MeCN (1 mM cat.), 0.1 M *n*-Bu_4NPF_6 electrolyte with a glassy carbon working electrode, platinum counter electrode, and platinum pseudoreference electrode with ferrocene as the internal standard. All of the scans are performed at 100 mV/s. i_{cat1} and i_{cat2} are the peak catalytic currents at the first and second reduction waves under a CO_2 atmosphere, respectively. i_p is the peak current under an N_2 atmosphere and is denoted as the first or second reduction peak. Given the deviation from ideal S-shaped curves in the cyclic voltammetry measurements, all $(i_{cat}/i_p)^2$ values and all TOF values are estimates of catalytic rates and are reported to a single significant figure throughout this Article.[34]

Cyclic voltammetry was performed under a CO_2 atmosphere to observe any catalytic current increases and to quantify the rates of the catalyst through comparison to peak current values (i_p) under inert atmosphere through the equation $(i_{cat}/i_p)^2$ where i_{cat} is the peak catalytic current value under CO_2 (Figure 3). The $(i_{cat}/i_p)^2$ term is used directly in the derived TOF equation where the remaining equation variables are constants and catalyst or substrate concentrations held constant. The calculated TOF values are reported in addition to the $(i_{cat}/i_p)^2$ values.[35] Despite relatively small shifts in reduction potentials across the catalyst series, the catalytic rates and curve shapes for CO_2 reduction varies significantly based on the NHC substituent. The highest catalytic rate is observed for the Re(pyNHC-$PhCF_3$)$(CO)_3$Br catalyst (**2**) with an $(i_{cat}/i_p)^2$ of 3 at the first and 4 at the second reduction wave. CO_2 reduction $(i_{cat}/i_p)^2$ values at the first reduction waves proceeded as follows: **2** > **5** > **4** ranging from 3 to only slightly catalytic at 2. The catalysts show modest changes in $(i_{cat}/i_p)^2$ values between the first and second reduction waves with catalyst **2** showing a significant increase from 3 to 4. Comparing catalysts **2** and **5** with benchmark catalyst **1**, the difference in overpotential at which catalysis occurs is very similar (<50 mV difference) even though both the first and the second reduction potential onsets vary by 300−350 mV. This is the result of catalysts **2**, **4**, and **5** all showing catalytic current increases at the first reduction wave, while benchmark catalyst **1** shows catalysis at the second reduction wave only. As catalyst **2** gave the highest $(i_{cat}/i_p)^2$ values in this series with a comparable CO_2 reduction overpotential, we selected this catalyst for more thorough electrochemical analysis with various protic additives (water, trifluoroethanol, phenol). CVs of **2** as a function of scan rate, under both N_2 and CO_2 atmospheres, confirm the diffusional nature of this system as peak currents are linear versus the square root of the scan rate (Figures S2−S5). Turnover frequencies (TOF) were determined for catalyst **2** from cyclic voltammetry in the presence of CO_2 and with added proton sources as previously described by Kubiak and co-workers.[35]

Given earlier reports regarding dimerization of Re bipyridyl catalysts, we examined catalysis with **2** as a function of catalyst concentration.[37] Catalytic current at both the first and the second reductions is linear versus [**2**], consistent with catalysis that is first order in Re complex (Figures S6 and S7). The reaction is presumed second order in acid based on previous studies of Re bipyridyl catalysts.[37,38]

Proton Source Evaluation: Phenol. Proton sources are known to enhance CO_2 reduction rates; however, controlling selectivity for reduction of CO_2 in the presence of H^+ is challenging for many catalysts. We chose to evaluate three acid sources via cyclic voltammetry with increasing acidity: water (H_2O, pK_{aaq} 15.7) < trifluoroethanol (TFE, pK_{aaq} 12.5) < phenol (PhOH, pK_{aaq} 10). To evaluate the effects of phenol on CO_2 reduction with catalyst **2**, cyclic voltammograms were taken under N_2 and CO_2 with increasing phenol concentrations over a range of 0−2 M (Figures 4 and S8). The first peak current values were found to increase significantly from no PhOH to 0.5 M PhOH before decreasing between 0.5 and 1.5 M in phenol, while the second reduction wave showed only modest changes in rate with increasing phenol concentration. The highest $(i_{cat}/i_p)^2$ value of 6 (TOF 1 s^{-1}) was observed at the first reduction potential with a peak rate at PhOH (0.5 M).

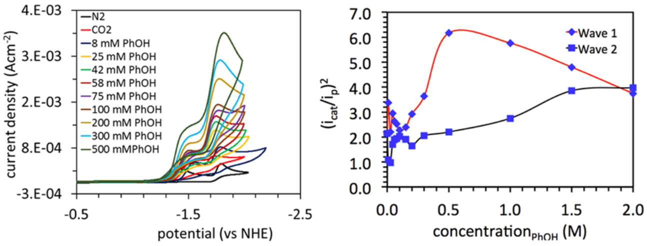

Figure 4. Left: Current density (A cm^{-2}) versus potential (V vs NHE) for catalyst **2** (1 mM) under nitrogen (black), under CO_2 (red), and under CO_2 with different concentrations of PhOH. Experiments performed in acetonitrile with 0.1 M *n*-Bu_4NPF_6 with a scan rate of 100 mV/s using a glassy carbon flat electrode, platinum counter electrode, and platinum pseudoreference electrode. Ferrocene is used as an internal standard. Right: $(i_{cat}/i_p)^2$ versus concentration of PhOH for the first reduction wave (red) and the second reduction wave (black), where i_p is the peak current at a reduction wave under N_2 at the same PhOH concentration as i_{cat}, which is the peak current at the same reduction wave under CO_2. See Figure S9 for CV sweeps at different concentrations of PhOH under N_2.

Controlled potential electrolysis (CPE) was performed to analyze the products formed with and without phenol (Table 2). CPE experiments were performed by setting the potential to that of the peak values observed via CV under a CO_2 atmosphere with a glassy carbon rod electrode. Without phenol, charge passed (C) was relatively slow at both the first (−1.41 V versus NHE) and the second (−1.67 V versus NHE) potentials, and maximum Faradaic efficiencies (FEs) during the first hour of electrolysis were 40% and 65%, respectively. As the electrolysis was observed to give a higher FE at the second reduction, PhOH concentrations were evaluated at the second reduction potentials. At 0.5 M PhOH, the rate of charge passing was only modestly affected when compared to no PhOH, and a similar peak FE was observed with some observed H_2 production (∼5% FE). However, 1.5 M PhOH concentration was observed to pass substantially more charge (13 C versus 2−3 C) with a lower FE for CO production (28% FE) and a dramatic increase in H_2 production (35% FE). As such, we rationalize the increase in current from the CV sweeps with PhOH was largely a result of increased H_2 production.

Proton Source Evaluation: TFE and H_2O. TFE and H_2O were evaluated via CV experiments to explore the influence of proton source on catalysis. With the addition of TFE, peak catalytic current was found to significantly increase over a wide range of TFE concentrations (from 0 to 1.1 M) and then decrease at higher concentrations of TFE (Figures 5 and S10). Both reduction wave current values were found to increase over the concentration of TFE up to ∼1 M before decreasing. After 2 M concentration, the catalytic activity dramatically decreases with the increasing TFE concentration. At the peak current passing rates, TFE passes charge at a significantly higher rate than with no additive (Table 3). 1.1 M TFE was selected for further experiments as peak catalytic current for both reduction waves occurred near this value. The scan rate dependence in CV experiments at 1.1 M TFE concentrations with **2** under both N_2 and CO_2 atmospheres confirms the diffusional nature of this system (Figures S10 and S11).

CPE experiments with 1.1 M TFE as an additive show a considerable increase in current passed (4 C with TFE vs 0.71 C with no additives) at the first reduction peak potential, consistent with CV experiments described above (Table 2). The product selectivity and efficiency is significantly improved from a peak FE of 40% (no additive) to 77% (with TFE). Only trace H_2 production was observed. This substantial, productive catalytic rate change and increase in Faradaic efficiency with the addition of TFE when compared to PhOH suggests high pK_a proton sources are beneficial for CO production. To evaluate this hypothesis, experiments with H_2O as the proton source were performed.

CV experiments with water additives show a remarkable increase in current at the first reduction wave between 0.77 M H_2O and 2.5 M H_2O before decreasing below the catalytic rate values observed in the absence of proton source (Figure 6). The CV curve shape shifts significantly as higher concentrations of water are added with an initial increase in current as an apparent shoulder at a potential similar to the first reduction potential and a shifting of the second reduction potential toward less negative potentials. At 2 M H_2O, the two waves have coalesced to give a dominant feature with only a negligible contribution from a more negative reduction peak. Given the overlap of these two waves, which could represent two distinct species in solution given the apparent shift in the second reduction wave, the simple selection of the highest current value at a given potential versus water concentration could be misleading as this curve peaks with 1 M H_2O, but represents the overlap of potentially two distinct species (Figure 6). As such, controlled potential electrolysis was analyzed at the 2 M H_2O concentration as this concentration has the highest observed current enhancement from what appears to be a single broad peak.

Figure 7 compares the CV curve shapes at arbitrary current values with no added proton source, 1.1 M TFE, and 2 M H_2O to clearly illustrate the influence of TFE primarily on the second reduction potential and the influence of H_2O at what appears to be the first reduction potential (see Table 3 for a rate comparison). The highest TOFs were observed at the first reduction potential with both 1.1 M TFE at 1 s^{-1} ($(i_{cat}/i_p)^2 = 7$) and with 1.2 M H_2O at 100 ($(i_{cat}/i_p)^2$ = 700). The second reduction wave was found to give lower TOF values for both TFE and H_2O at each concentration of proton source examined

DOI: 10.1021/acs.inorgchem.6b00626

Table 2. Control Potential Electrolysis of **2** and **1** at Different Potentials with Varying Proton Sources[a]

catalyst	additive	potential [V vs NHE] (wave)	time [min]	charge [C]	FE_{CO} % (FE_{H2} %)
2	none	−1.41(1)	20	0.22	40
			40	0.45	40
			60	0.71	27
2	none	−1.67(2)	20	0.96	60
			40	2.00	65
			60	2.92	62
2	0.5 M PhOH	−2.01(2)	20	0.98	65(5)
			40	1.52	47(4)
			60	2.25	37(3)
2	1.5 M PhOH	−2.21(2)	20	4.72	28(35)
			40	10.03	25(35)
			60	13.02	21(33)
2	1.1 M TFE	−1.51(1)	20	1.37	61
			40	2.60	77
			60	4.16	43
2	2 M H_2O	−1.41(1)	20	1.06	89
			40	2.15	78
			60	3.32	66
2	2 M H_2O	−1.86(2)	20	10.74	102
			40	12.56	95
			60	13.30	92
Re(bpy)$(CO)_3$Br	none	−1.31(2)	20	0.97	87
			40	1.70	61
			60	2.11	51
Re(bpy)$(CO)_3$Br	2 M H_2O	−1.31(2)	20	1.39	83
			40	2.28	73
			60	2.79	61

[a] Electrolysis reactions were run in MeCN with 0.1 M *n*-Bu_4NPF_6 as electrolyte with a type 2 glassy carbon rod as the working electrode, a Ag/AgCl reference electrode, and a platinum foil sheet as the counter electrode in a fine glass fritted isolation chamber and a catalyst concentration of 1 mM. The isolation chamber solution consisted of the same concentration of electrolyte in MeCN with added ferrocene as a sacrificial oxidant. Electrolysis were run for 1 h. The electrolysis potentials are selected from pre-electrolysis reaction mixture CVs with the controlled potential electrolysis electrodes at the peak of the wave being analyzed. Catalyst concentration was 1 mM in all cases.

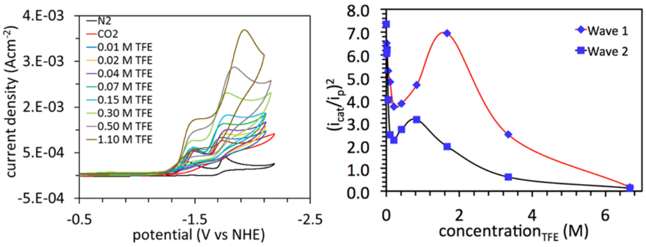

Figure 5. Left: Current density (A cm^{-2}) versus potential (V vs NHE) plots with catalyst **2** (1 mM) in total amount of solvent with 0.1 M *n*-Bu_4NPF_6 in acetonitrile under nitrogen (black), under CO_2 (red), and under CO_2 with different concentrations of TFE and a scan rate of 100 mV/s. Right: $(i_{cat}/i_p)^2$ versus concentration of TFE, where i_p is the peak current at a reduction wave under N_2 at the same concentration of TFE (Figure S12) as the peak current at the same reduction wave under CO_2 (i_{cat}). Experiments were performed using a glassy carbon flat electrode, platinum counter electrode, and platinum pseudoreference electrode. Ferrocene was used as an internal standard.

when N_2 versus CO_2 current values were compared at the same concentration of additive (Figures S12 and S13). Further studies will be needed to better understand this substantial change in rate; however, a new peak is apparent via CV between the potential of the first and second reductions of the catalyst in the presence of water, and attributing this substantial current increase to the first reduction of **2** alone should be cautioned.

Table 3. Rates for Electrocatalytic CO_2 Reduction with **2** and Various Proton Sources[a]

proton source	$[H^+]$ (M)	$(i_{cat}/i_p)^2$ peak 1	TOF (s^{-1}) peak 1	$(i_{cat}/i_p)^2$ peak 2	TOF (s^{-1}) peak 2
none		3	0.7	4	0.8
TFE	1.1	7	1	2	0.4
H_2O	1.2	700	100	400	80
H_2O	2	200	30	30	5

[a] All peak currents obtained from CVs with 100 mV/s scan rate in acetonitrile with 1 mM catalyst **2** concentration. Experiments performed in acetonitrile with 0.1 M *n*-Bu_4NPF_6 with a scan rate of 100 mV/s using a glassy carbon flat electrode, platinum counter electrode, and platinum pseudoreference electrode. Ferrocene is used as an internal standard.

Attempts to determine a CO_2 binding constant, K_{CO2}, via electrochemistry were unsuccessful. In limited cases, specifically Co and Ni macrocycles, a significant shift in reduction potentials is observed as a function of CO_2 concentration, allowing K_{CO2} to be found.[39,40] However, minimal or no apparent shift was observed in cyclic voltammograms under N_2 versus CO_2 with our Re catalysts. Others have determined binding constants, again, for Co macrocycles with pulse-radiolysis experiments[41] and transient absorption spectroscopy.[13] Indeed, the Co macrocyclic systems are amenable to these measurements as even catalyst intermediates have been characterized by X-ray crystallography.[42] In light of these

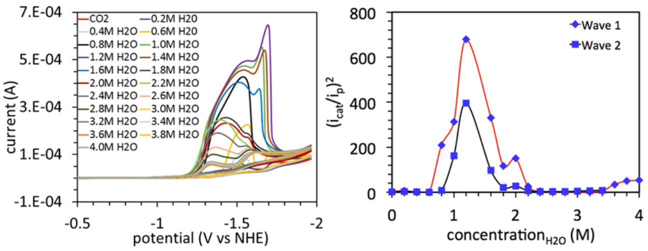

Figure 6. Left: Current (A) versus potential (V vs NHE) cyclic voltammograms for catalyst **2** (1 mM) under CO_2 with different concentrations of H_2O. Experiments performed in acetonitrile with 0.1 M n-Bu_4NPF_6 with a scan rate of 100 mV/s using a glassy carbon disk electrode, platinum counter electrode, and platinum pseudoreference electrode. Ferrocene is used as an internal standard. Right: $(i_{cat}/i_p)^2$ versus concentration of H_2O, where i_p is the peak current at a reduction wave under N_2 at the same concentration of H_2O (Figure S13) as the peak current at the same reduction wave under CO_2 (i_{cat}).

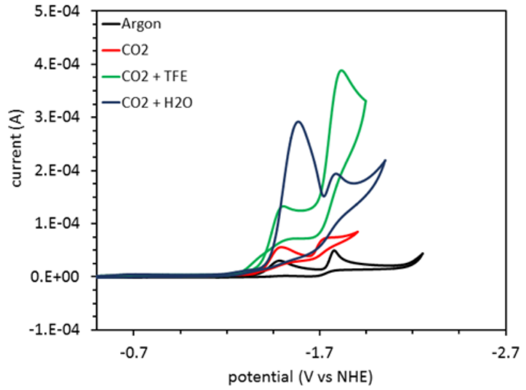

Figure 7. Cyclic voltammograms at 100 mV/s scan rate of 1 mM **2** under argon and carbon dioxide atmosphere in 0.1 M $TBAPF_6$/MeCN. TFE (1.1 M) and H_2O (2 M) were used as a proton sources. A glassy carbon working electrode was used with a platinum wire counter electrode. A platinum wire was also used as a quasi-reference electrode. Ferrocene was added as an internal standard.

observations, we performed additional experiments at 2 M H_2O to analyze just the species reduced at less negative overpotentials, which appears as a broad wave substantially larger than the second reduction wave.

Current versus scan rate dependence shows a typical current increase response under both argon and CO_2 as scan rate increases (Figure S13). However, due to the substantial increase in a new species in solution, analysis of scan rate dependence to show the diffusional nature of this system is confounded. To evaluate the product distribution and FE at 2.0 M H_2O concentrations, CPE experiments were performed (Table 2). At the peak current potential via CV (−1.41 V), CPE was measured to show only a slight increase in current passed (3 C at the first hour) when compared to no water additive; however, a substantial improvement in peak FE was observed (89% versus 40% for no additive and 77% for TFE). In all experiments involving H_2O, only trace H_2 was observed. Adjusting the CPE potential to −1.86 V (the potential of the minor second reduction wave in 2 M H_2O), the charge passed increases dramatically to 13 C in the first hour. We note that of the 13.3 C passed in 60 min at this potential, 10.7 C was within the first 20 min where the FE_{CO} was measured at ∼100%. Despite the significant change in charge passed between the 20 and 60 min time points, the FE only slightly diminishes to 92%.

Having established H_2O as a current-enhancing additive, which results in minimal catalyst deactivation for **2**, we sought to compare CPE studies of **2** and benchmark catalyst $Re(bpy)(CO)_3Br$ to evaluate FEs and determine product distributions. CPE was performed with catalyst **2** at the first and second peak reduction potentials with and without water (Figure 8, Table 2), and compared to CPE experiments with $Re(bpy)(CO)_3Br$ at the peak CO_2 reduction potential with and without water (Table 2).

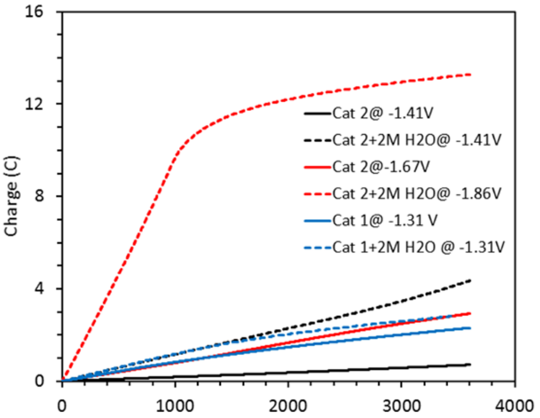

Figure 8. Charge passed over the time during the controlled potential electrolysis experiments of catalyst **2** (black, reduction peak 1; and red, reduction peak 2) and the benchmark catalyst (catalyst **1**, blue). Solid lines are electrolysis without water, and dashed lines are with 2 M H_2O. All catalyst concentrations are 1 mM. Electrolysis reactions were run in MeCN with 0.1 M n-Bu_4NPF_6 as electrolyte with a type 2 glassy carbon rod as the working electrode, a Ag/AgCl reference electrode, and a platinum foil sheet as the counter electrode in a fine glass fritted isolation chamber and a catalyst concentration of 1 mM. The isolation chamber solution consists of the same concentration of electrolyte in MeCN with added ferrocene as a sacrificial oxidant. Electrolysis were run for 1 h. The electrolysis potentials are selected from pre-electrolysis reaction mixture CVs with the controlled potential electrolysis electrodes at the peak of the wave being analyzed.

For benchmark catalyst $Re(bpy)(CO)_3Br$, the charge passed and Faradaic efficiency for CO production (FE_{CO}) after 1 h reached 2.11 C passed and 51% FE_{CO} with an applied potential of −1.31 V vs NHE (Figure 8, Table 2). Under the same experimental conditions, catalyst **2** gives 0.71 C passed at 27% FE_{CO} at −1.41 V vs NHE at the first reduction wave and 2.92 C passed with 62% FE at a fixed potential of −1.67 V vs NHE at the second reduction wave (Table 2). In general, FE was found to decrease significantly as a function of time under these relatively dry conditions, while accumulated charge passed remains nearly linear with time. Upon addition of 2 M H_2O relative to the catalyst, the current density and Faradaic efficiencies improve for the benchmark catalyst and **2**, with more dramatic effects observed for catalyst **2**. Specifically, the benchmark catalyst, $Re(bpy)(CO)_3Br$, shows only a slight enhancement in charge passed (2.79 C vs 2.11 C) and a modest increase in FE_{CO} (61% vs 51%) with 2 M H_2O and an applied potential of −1.31 V vs NHE. Significantly, catalyst **2** also shows a dramatic increase in charge passed at the first reduction potential (3.32 C vs 0.71 C) with a large increase in FE_{CO} (66% vs 27% at 1 h) in the presence of H_2O at −1.41 V vs NHE (first reduction wave). The increase in catalyst performance is further enhanced at the second reduction wave (−1.81 V vs NHE), exhibiting 13.3 C versus 2.92 C and 92% versus 62% FE at 1 h

DOI: 10.1021/acs.inorgchem.6b00626
Inorg. Chem. XXXX, XXX, XXX−XXX

of electrolysis versus no additive. These charge passing rates are graphically illustrated in Figure 8.

To probe the sudden drop in charge passed by **2** during electrolysis in the presence of 2 M H_2O at the second reduction wave, we addressed the following concerns: (1) has the sacrificial oxidant (ferrocene/electrolyte) been depleted in the counter electrode isolation chamber, (2) has the CO_2 concentration in solution dropped dramatically, (3) has the catalyst been deactivated by CO poisoning, or (4) has nonlinear catalyst degradation occurred (Figure 9). We first ran a CPE until the drastic change in activity had occurred, then refreshed the ferrocene/electrolyte in the counter electrode chamber, which did not restore activity. CO_2 was then freshly purged through the solution to replenish dissolved CO_2 and to reduce the concentration of CO; however, again initial activity was not restored.[43] To examine any change in catalyst structure, UV−vis absorption spectroscopy was employed to compare the reaction mixture before and after CPE. As catalyst **2** is a known photocatalyst with visible light, the lowest energy absorptions in the working electrode compartment mixture are attributed to **2**. Prior to electrolysis, the reaction mixture absorption curve matches that of pure **2** in acetonitrile from 350 to 450 nm. After the electrolysis, the MLCT absorption band at 350 nm is nearly gone, and a new absorption peak at ∼315 nm has grown in. Additionally, a lower energy absorption band in the pre-electrolyzed solution (∼400 nm, shoulder) has substantially shifted toward longer wavelengths to 450 nm (Figure 10). The acetonitrile was removed via vacuum, and the crude solids (decomposed catalyst, byproducts, and electrolyte) were analyzed by ^{1}H NMR, revealing a shift of the NMR peaks in the aromatic region (Figure S14). A similar approach to evaluating the change in the structure of **2** has been done by Massi et al. on structurally analogous Re-PyNHC complexes after photoexcitation rather than electrolysis. His study shows that the complex may undergo loss of a CO ligand upon irradiation in MeCN.[29] However, in our case, the changes in the UV−vis absorption spectrum are substantially different from those previously observed, suggesting another deactivation pathway for **2** may be in play such as catalyst dimerization as recently elucidated through interesting work by Agarwal et al.[44]

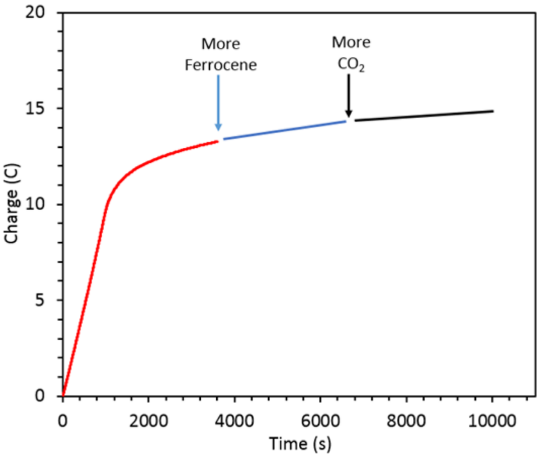

Figure 9. Charge (C) passed over the time (s) during the electrolysis of catalyst **2** (1 mM) at −2.05 V (vs SCE) (0.1 M $TBAPF_6$ in MeCN, and 2 M H2O). Red line: Electrolysis with Figure 8 conditions. Blue line: Continued electrolysis with the same reaction and refreshed ferrocene in the isolation chamber. Black line: Continued electrolysis with the same reaction after refreshing the solution with CO_2.

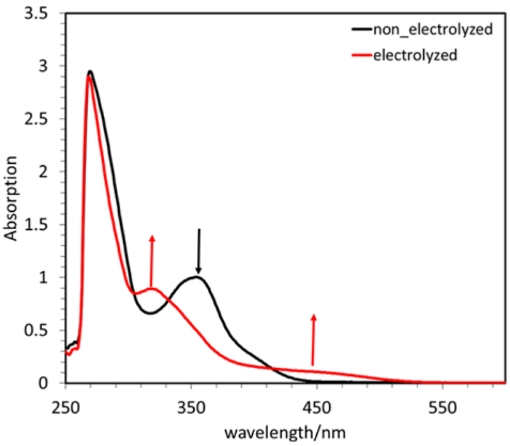

Figure 10. UV−vis absorption spectrum for the catalyst **2** prior to electrolysis as performed in Figure 9 (black) and upon completion of the electrolysis performed in Figure 9 (red).

The rate of catalysis has clearly been dramatically enhanced with the addition of a proton source with substantial catalysis occurring at the first reduction wave. A potential mechanistic pathway to explain these observations is provided (Figure 11).

Mechanistic species **1** may first be reduced to give the anionic complex **2**, which may dissociate an anionic ligand to give neutral 17 electron complex **3**. **3** then may nucleophilically add to CO_2 by providing an additional electron from the electron-rich NHC ligand to give a ligand centered cation **4** (shown as the inset). On the basis of the absence or presence of a proton source, **4** may add either CO_2 or H^+ to the carboxylate group and accept an electron to give either **5** or **7**, respectively. Release of carbonate from **5** gives cationic complex **6**, which upon reduction and CO dissociation regenerates catalyst **3**. Alternatively, complex **7** may undergo proton assisted water release to give the same cationic intermediate **6** as proposed under aprotic conditions. Attempts to observe reaction pathway intermediates to either validate or refine this mechanistic hypothesis are presently ongoing.

■ CONCLUSIONS

We have synthesized three new $Re(pyNHC)(CO)_3Br$ catalysts by substituting the $-CF_3$ group of $Re(pyNHC\text{-}PhCF_3)(CO)_3Br$ with a series of electron-withdrawing groups. The effects of these substitutions were compared to $Re(pyNHC\text{-}PhCF_3)(CO)_3Br$ (**2**) and benchmark catalyst ($Re(bpy)(CO)_3Br$) as electrocatalysts for the reduction of CO_2 to CO. The pyNHC catalysts were shown to reduce CO_2 at the first reduction wave rather than only at the second reduction wave as was observed for the bipyridyl based catalyst **1**. Among the series of pyNHC-catalysts, $Re(pyNHC\text{-}PhCF_3)(CO)_3Br$ (**2**) showed the most promising results as an electrocatalyst through $(i_{cat}/i_p)^2$/TOF rate analysis. The electrocatalytic performance of **2** was evaluated by cyclic voltammetry with a variety of proton sources including PhOH, TFE, and H_2O with controlled potential electrolyses performed for product analysis. The catalytic rate $(i_{cat}/i_p)^2$/TOF for CO_2 reduction by catalyst **2** was found to be 3/0.7 s^{-1} (first wave) and 4/0.8 s^{-1} (second wave) without an added proton source. Through the addition of H_2O, this rate could be enhanced up to a TOF of 100 s^{-1} ($(i_{cat}/i_p)^2$ = 700) at a potential energetically corresponding to the first

DOI: 10.1021/acs.inorgchem.6b00626
Inorg. Chem. XXXX, XXX, XXX−XXX

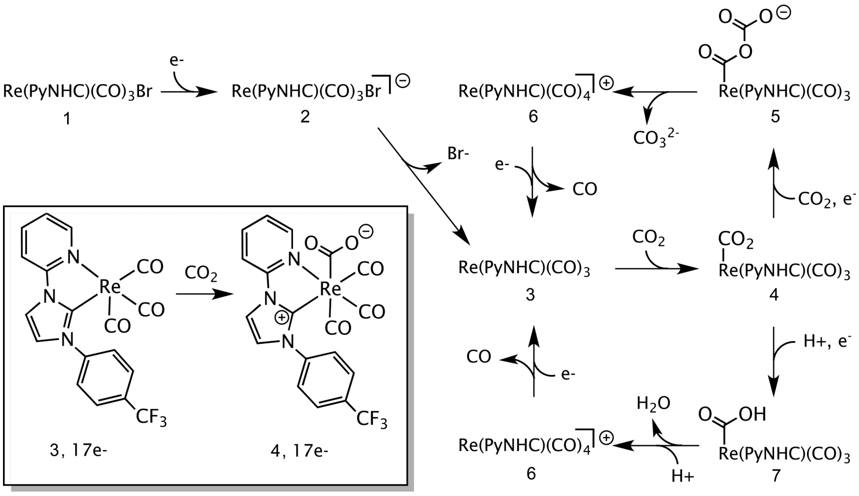

Figure 11. A proposed mechanism where catalytic activity may occur after the first reduction and a difference in mechanistic pathways resulting from proton source addition.

reduction of **2**. Controlled potential electrolysis (CPE) studies show addition of PhOH produces significant quantities of H_2, while TFE and H_2O gave only trace H_2. Under conditions without an added proton source, **2** demonstrates improved results FE% (62%) as compared to benchmark catalyst (Re(bpy)$(CO)_3$Br) at 51% FE. Moreover, we were able to optimize the catalytic performance by using H_2O as an additive to facilitate the proton-coupled conversion of CO_2 to CO. In the presence of water as the proton source, we measured a 92% FE for CO production with catalyst **2** and 61% FE for the benchmark Re-bipyridyl catalyst at 1 h. A peak FE% was observed at 100% during early time points. To the best of our knowledge, this represents a significant improvement in FE% for transition metal ligated PyNHC triscarbonyl complexes, which have typically given FE% near 60%. A significant change in the rate of catalysis was observed with H_2O as an additive during CPE. Refreshing reaction reactants did not restore the original charge passing rate, and a clear change in the UV−vis absorption and chemical shifts in NMR was observed for catalyst **2** before and after electrolysis. Experiments attempting to elucidate the change in catalyst structure that occurs during electrolysis are ongoing.

■ ASSOCIATED CONTENT

Ⓢ Supporting Information

The Supporting Information is available free of charge on the ACS Publications website at DOI: 10.1021/acs.inorgchem.6b00626.

Experimental procedures, CV scans, and ^{1}H NMR spectra (PDF)

■ AUTHOR INFORMATION

Corresponding Authors

*E-mail: jwjurss@olemiss.edu.
*E-mail: delcamp@olemiss.edu.

Notes

The authors declare no competing financial interest.

■ ACKNOWLEDGMENTS

N.P.L., H.A.D., A.J.H., J.W.J., and J.H.D. thank NSF (NSF OIA-1539035). H.A.D. and J.W.J. thank the University of Mississippi for funding.

■ REFERENCES

(1) Aresta, M.; Dibenedetto, A.; Angelini, A. *Chem. Rev.* **2014**, *114*, 1709.
(2) Underwood, A. J. V. *Ind. Eng. Chem.* **1940**, *32*, 449.
(3) Smieja, J. M.; Kubiak, C. P. *Inorg. Chem.* **2010**, *49*, 9283.
(4) Xiaoding, X.; Moulijn, J. A. *Energy Fuels* **1996**, *10*, 305.
(5) Mikkelsen, M.; Jørgensen, M.; Krebs, F. C. *Energy Environ. Sci.* **2010**, *3*, 43.
(6) Benson, E. E.; Kubiak, C. P.; Sathrum, A. J.; Smieja, J. M. *Chem. Soc. Rev.* **2009**, *38*, 89.
(7) Savéant, J. M. *Chem. Rev.* **2008**, *108*, 2348.
(8) Appel, A. M.; Bercaw, J. E.; Bocarsly, A. B.; Dobbek, H.; DuBois, D. L.; Dupuis, M.; Ferry, J. G.; Fujita, E.; Hille, R.; Kenis, P. J.; Kerfeld, C. A.; Morris, R. H.; Peden, C. H.; Portis, A. R.; Ragsdale, S. W.; Rauchfuss, T. B.; Reek, J. N.; Seefeldt, L. C.; Thauer, R. K.; Waldrop, G. L. *Chem. Rev.* **2013**, *113*, 6621.
(9) Yui, T.; Tamaki, Y.; Sekizawa, K.; Ishitani, O. *Top. Curr. Chem.* **2011**, *303*, 151.
(10) Schneider, J.; Jia, H.; Muckerman, J. T.; Fujita, E. *Chem. Soc. Rev.* **2012**, *41*, 2036.
(11) Huckaba, A. J.; Sharpe, E. A.; Delcamp, J. H. *Inorg. Chem.* **2016**, *55*, 682.
(12) Chen, Z.; Concepcion, J. J.; Brennaman, M. K.; Kang, P.; Norris, M. R.; Hoertz, P. G.; Meyer, T. J. *Proc. Natl. Acad. Sci. U. S. A.* **2012**, *109*, 15606.
(13) Ogata, T.; Yanagida, S.; Brunschwig, B. S.; Fujita, E. *J. Am. Chem. Soc.* **1995**, *117*, 6708.
(14) Costentin, C.; Drouet, S.; Robert, M.; Saveant, J. M. *Science* **2012**, *338*, 90.
(15) Thoi, V. S.; Chang, C. J. *Chem. Commun.* **2011**, *47*, 6578.
(16) Froehlich, J. D.; Kubiak, C. P. *Inorg. Chem.* **2012**, *51*, 3932.
(17) Angamuthu, R.; Byers, P.; Lutz, M.; Spek, A. L.; Bouwman, E. *Science* **2010**, *327*, 313.
(18) Bourrez, M.; Molton, F.; Chardon-Noblat, S.; Deronzier, A. *Angew. Chem., Int. Ed.* **2011**, *50*, 9903.
(19) Sampson, M. D.; Nguyen, A. D.; Grice, K. A.; Moore, C. E.; Rheingold, A. L.; Kubiak, C. P. *J. Am. Chem. Soc.* **2014**, *136*, 5460.
(20) Agarwal, J.; Shaw, T. W.; Stanton, C. J., III; Majetich, G. F.; Bocarsly, A. B.; Schaefer, H. F., III. *Angew. Chem., Int. Ed. Engl.* **2014**, *53*, 5152.

(21) Jupally, V. R.; Dharmaratne, A. C.; Crasto, D.; Huckaba, A. J.; Kumara, C.; Nimmala, P. R.; Kothalawala, N.; Delcamp, J. H.; Dass, A. *Chem. Commun.* **2014**, *50*, 9895.

(22) Sheng, M.; Jiang, N.; Gustafson, S.; You, B.; Ess, D. H.; Sun, Y. *Dalton. Trans.* **2015**, *44*, 16247.

(23) Kang, P.; Chen, Z.; Nayak, A.; Zhang, S.; Meyer, T. J. *Energy Environ. Sci.* **2014**, *7*, 4007.

(24) Agarwal, J.; Shaw, T. W.; Schaefer, H. F., III; Bocarsly, A. B. *Inorg. Chem.* **2015**, *54*, 5285.

(25) Therrien, J. A.; Wolf, M. O.; Patrick, B. O. *Inorg. Chem.* **2014**, *53*, 12962.

(26) Fuertes, S.; Chueca, A. J.; Sicilia, V. *Inorg. Chem.* **2015**, *54*, 9885.

(27) Alakonda, L.; Periasamy, M. *Synthesis* **2012**, *44*, 1063.

(28) Vaughan, J. G.; Reid, B. L.; Ramchandani, S.; Wright, P. J.; Muzzioli, S.; Skelton, B. W.; Raiteri, P.; Brown, D. H.; Stagni, S.; Massi, M. *Dalton. Trans.* **2013**, *42*, 14100.

(29) Vaughan, J. G.; Reid, B. L.; Wright, P. J.; Ramchandani, S.; Skelton, B. W.; Raiteri, P.; Muzzioli, S.; Brown, D. H.; Stagni, S.; Massi, M. *Inorg. Chem.* **2014**, *53*, 3629.

(30) Chan, C. Y.; Pellegrini, P. A.; Greguric, I.; Barnard, P. J. *Inorg. Chem.* **2014**, *53*, 10862.

(31) Pegis, M. L.; Roberts, J. A.; Wasylenko, D. J.; Mader, E. A.; Appel, A. M.; Mayer, J. M. *Inorg. Chem.* **2015**, *54*, 11883.

(32) Roberts, J. A.; Bullock, R. M. *Inorg. Chem.* **2013**, *52*, 3823.

(33) Appel, A. M.; Helm, M. L. *ACS Catal.* **2014**, *4*, 630.

(34) Rountree, E. S.; McCarthy, B. D.; Eisenhart, T. T.; Dempsey, J. L. *Inorg. Chem.* **2014**, *53*, 9983.

(35) Smieja, J. M.; Sampson, M. D.; Grice, K. A.; Benson, E. E.; Froehlich, J. D.; Kubiak, C. P. *Inorg. Chem.* **2013**, *52*, 2484.

(36) Connelly, N. G.; Geiger, W. E. *Chem. Rev.* **1996**, *96*, 877.

(37) Machan, C. W.; Chabolla, S. A.; Yin, J.; Gilson, M. K.; Tezcan, F. A.; Kubiak, C. P. *J. Am. Chem. Soc.* **2014**, *136*, 14598.

(38) Wong, K.-Y.; Chung, W.-H.; Lau, C.-P. *J. Electroanal. Chem.* **1998**, *453*, 161.

(39) Schmidt, M. H.; Miskelly, G. M.; Lewis, N. S. *J. Am. Chem. Soc.* **1990**, *112*, 3420.

(40) Fujita, E.; Creutz, C.; Sutin, N.; Szalda, D. J. *J. Am. Chem. Soc.* **1991**, *113*, 343.

(41) Creutz, C.; Schwarz, H. A.; Wishart, J. F.; Fujita, E.; Sutin, N. *J. Am. Chem. Soc.* **1991**, *113*, 3361.

(42) Fujita, E.; Szalda, D. J.; Creutz, C.; Sutin, N. *J. Am. Chem. Soc.* **1988**, *110*, 4870.

(43) Froehlich, J. D.; Kubiak, C. P. *J. Am. Chem. Soc.* **2015**, *137*, 3565.

(44) Stanton, C. J., 3rd; Machan, C. W.; Vandezande, J. E.; Jin, T.; Majetich, G. F.; Schaefer, H. F., 3rd; Kubiak, C. P.; Li, G.; Agarwal, J. *Inorg. Chem.* **2016**, *55*, 3136.

DOI: 10.1021/acs.inorgchem.6b00626
Inorg. Chem. XXXX, XXX, XXX−XXX